

Investigation of modulation characteristics of high speed InGaAs/GaAs double state lasing quantum dot lasers

FARZANEH KARIMINEZHAD, ESFANDIAR RAJAEI*

Department of Physics, University of Guilan, Rasht, Iran

A theoretical analysis of the high-speed characteristics of InGaAs/GaAs quantum dot (QD) lasers is presented. Both the ground and excited states small signal frequency responses are obtained by analysing small signal modulation. The rate equations for the electrons, holes and photons are solved numerically using the fourth-order Runge-Kutta method. The effect of relaxation time on light – current characteristics is presented. Modulation response and 3-dB modulation bandwidth in various injected current densities, capture times and laser cavity lengths are investigated. Some analytical expressions are derived that indicate the relationship between these characteristics and modulation bandwidth. The present results show how the dynamics of electrons and holes improve the excited state lasing and high-speed modulation of laser.

(Received February 20, 2015; accepted June 09, 2016)

Keywords: InGaAs/GaAs quantum dot laser, Small signal modulation, Modulation frequency response

1. Introduction

Semiconductor quantum dot (QD) lasers use QDs as the active medium and show superior characteristics over traditional bulk, quantum well (QW) and quantum wire (QWR) lasers. This is due to the three-dimensional confinement for carriers with atom-like energy levels. These characteristics are low threshold current [1], temperature insensitivity [2], low chirp [3], and 1.3 and 1.55 μm emission wavelengths suitable for telecommunication applications [4]. Direct modulation of QD plays a main role in optimization of optical communications; they are commonly used in optical fiber links because of their low cost, compressed size and low power requirements. There is a need to improve the high speed modulation characteristics of QD lasers. Possible methods are the use of tunnel injection, p-doped and excited state (ES) lasers. Theoretical [5-13] and experimental [14-15] studies have examined high speed modulation and bandwidth limitations for QD lasers. The dynamic properties of QD lasers have been investigated using models that have simulated their modulation response. A maximum modulation bandwidth of 7 GHz was obtained by Zhang et al. [16-17], but it was limited by QD carrier capture and relaxation time. Naderi has obtained the best modulation bandwidth of 12 GHz when examining the effect of capture time from the wetting layer (WL) to the ground state (GS) [18], but this value is still below those reported for QW lasers. Tong et al. have reported a bandwidth larger than 12 GHz for p-doped QD lasers operating at 1300 nm in wavelength [19], which is far below theoretical predictions [20].

It is necessary to improve modulation response and bandwidth.

The present study is developed a model for InGaAs/GaAs double-state QD laser. This model includes two discrete energy levels for electrons and one for holes

using all possible relaxation and escape paths and separate electron-hole dynamics [21]. Based on the rate equations model MATLAB software was used for the simulation. The small signal modulation (SSM) responses for the GS and ES were calculated. The modulation bandwidth, relaxation oscillation frequency and damping factor were extracted of the modulation response equations. The effect of inter-level relaxation time on light-current specifications for the GS and ES were investigated. The GS and ES SSM responses as a function of injected current density were plotted at different cavity lengths. SSM responses for four capture times from the WL to the GS and ES were simulated also. Increase of the modulation bandwidth by varying the capture time, cavity length and relaxation time was discussed. Optimization of the relaxation oscillation frequency and damping factor as a function of injected current density were presented. To our knowledge for the first time, we are calculated and simulated SSM response, relaxation oscillation frequency and damping factor of InGaAs/GaAs quantum dot laser by considering ES.

2. Model description

To study the dynamic of quantum dot laser, the energy band diagram for InGaAs/GaAs double-state QD laser that developed in [21] is applied and illustrated in fig. 1. This model is composed of conduction and valence bands with the WL and QD levels. The WL is considered as the reservoir of carriers to the lower energy states in QDs: the electron excited state (NES), electron ground state (NGS) and hole ground state (PGS) with four, two and six-fold degeneracies respectively. The QDs are considered to be neutral always which electrons and holes are treated as electron-hole pairs. The energy states are excitonic, dynamics of electrons and holes are separated quite. There

are some injected carriers into a separate confinement hetero-structure (SCH) barrier firstly and is assumed to be injected directly to the WL reservoir.

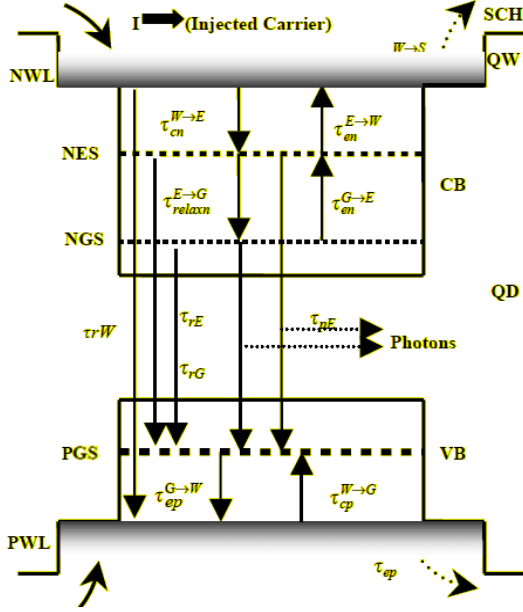


Fig. 1. Sketch of the carrier dynamics model.

They are captured to the ES with the capture time $\tau_{cn}^{W \rightarrow E}$ and then relax from the ES to the GS within a time $\tau_{relaxn}^{E \rightarrow G}$. Electrons can come back from the GS to the ES in a time of $\tau_{en}^{G \rightarrow E}$ and escape into the WL within time $\tau_{en}^{E \rightarrow W}$. Following the sketch of figure 1, the seven coupled rate equations on carrier and photon densities are:

$$\frac{df_{eWL}}{dt} = \frac{\eta_w J}{eN_c} - \frac{f_{eWL}}{\tau_{en}^{W \rightarrow S}} - \frac{f_{eWL}(1-f_{eES})}{\tau_{cn}^{W \rightarrow E}} + \frac{4N_d}{N_c} \frac{f_{eES}(1-f_{eWL})}{\tau_{en}^{E \rightarrow W}} - \frac{f_{eWL}f_{pWL}}{\tau_{rW}}, \quad (1)$$

$$\frac{df_{eES}}{dt} = \frac{N_c}{4N_d} \frac{f_{eWL}(1-f_{eES})}{\tau_{cn}^{W \rightarrow E}} - \frac{f_{eES}(1-f_{eWL})}{\tau_{en}^{E \rightarrow W}} - \frac{f_{eES}(1-f_{eGS})}{\tau_{relaxn}^{E \rightarrow G}} - 3s_{ES}(f_{eES} + f_{pGS} - 1) + \frac{f_{eGS}(1-f_{eES})}{2\tau_{en}^{G \rightarrow E}} - \frac{6f_{eES}f_{pGS}}{\tau_{rE}}, \quad (2)$$

$$\frac{df_{eGS}}{dt} = \frac{2f_{eES}(1-f_{eGS})}{\tau_{relaxn}^{E \rightarrow G}} - \frac{f_{eGS}(1-f_{eES})}{\tau_{en}^{G \rightarrow E}} - 3s_{GS}(f_{eGS} + f_{pGS} - 1) - \frac{6f_{eGS}f_{pGS}}{\tau_{rG}}, \quad (3)$$

$$\frac{df_{pGS}}{dt} = \frac{N_v}{6N_d} \frac{f_{pWL}(1-f_{pGS})}{\tau_{cp}^{W \rightarrow G}} - \frac{f_{pGS}(1-f_{pWL})}{\tau_{ep}^{G \rightarrow W}} - \frac{2f_{pGS}f_{eGS}}{\tau_{rG}} - \frac{4f_{pGS}f_{eES}}{\tau_{rW}} - s_{GS}(f_{eGS} + f_{pGS} - 1) - 2s_{ES}(f_{eES} + f_{pGS} - 1), \quad (4)$$

$$\frac{ds_{GS}}{dt} = \frac{6N_d}{S_{GS0}} s_{GS}(f_{eGS} + f_{pGS} - 1) + \beta \frac{f_{eGS}f_{pGS}}{\tau_{rG}} \frac{12N_d}{S_{GS0}} - \frac{s_{GS}}{\tau_{pG}}, \quad (5)$$

$$\frac{ds_{ES}}{dt} = \frac{12N_d}{S_{ES0}} s_{ES}(f_{eES} + f_{pGS} - 1) + \beta \frac{f_{eES}f_{pGS}}{\tau_{rE}} \frac{24N_d}{S_{ES0}} - \frac{s_{ES}}{\tau_{pE}}, \quad (6)$$

Charge neutrality is held in the whole system that is given as a relation (7):

$$\frac{N_v f_{pWL}}{2N_d} + 3f_{pGS} = \frac{N_c f_{eWL}}{2N_d} + f_{eGS} + 2f_{eES}. \quad (7)$$

Where f_{eWL} , f_{eES} and f_{eGS} are conduction band electron occupation probabilities in WL, ES and GS respectively. f_{pWL} and f_{pGS} are hole occupation probabilities in WL and GS of the valence band. s_{GS} and s_{ES} are normalized photon densities in the cavity with GS and ES resonance energy that is given by:

$$s_{G(E)S} = S_{G(E)S} / S_{G(E)S0}. \quad (8)$$

Where $S_{GS0} = 6N_d / v_g (\Gamma g_{GS})_{sat}$ and $S_{ES0} = 12N_d / v_g (\Gamma g_{ES})_{sat}$ are the photon densities while stimulated recombination lifetime of GS or ES is considered 2ns. $(\Gamma g_{GS})_{sat}$, $(\Gamma g_{ES})_{sat}$ and v_g are GS saturated modal gain, ES saturated modal gain and group velocity respectively. N_c, N_v are the effective densities of states in the WL conduction and valence bands. N_d is the QD areal density and β is spontaneous emission factor. The GS and ES photon lifetime is written as follows:

$$\frac{1}{\tau_{pE(G)}} = v_g [\alpha_{iE(G)} + \ln(\frac{1}{R_1 R_2}) / L], \quad (9)$$

Where R_1 and R_2 are cavity mirror reflectivities, L is the cavity and $\alpha_{iE(G)}$ is internal loss. The output power of QD laser can be expressed as:

$$P_{G(E)S} = s_{G(E)S} S_{G(E)S0} W L h \nu_{G(E)S} v_g \alpha_m, \quad (10)$$

Here, W is stripe width, $h \nu_{G(E)S}$ is the emitted GS or ES photon energy. Mirror loss is calculated by the following relation:

$$\alpha_m = \ln(1/R_1 R_2) / 2L. \quad (11)$$

The parameters used in QDL model are listed in table 1 [21-25].

Table 1

Parameter	Value	Unit
Injected efficiency, η_w	77%	
Cavity mirror reflectivities, $R_1 = R_2$	0.31	
Areal density of QDs, N_d	4.5×10^{21}	cm^{-2}
Internal loss, $\alpha_{iG} = \alpha_{iE}$	2	cm^{-1}
Temperature, T	295	K
Spontaneous emission factor, β	10^{-4}	
GS saturated modal gain, $(\Gamma g_{GS})_{sat}$	15	cm^{-1}
ES saturated modal gain, $(\Gamma g_{ES})_{sat}$	30	cm^{-1}
GS emitted photon energy, $h \nu_{GS}$	0.96	eV
ES emitted photon energy, $h \nu_{ES}$	1.04	eV
Electrons capture time from the WL into the ES, $\tau_{cn}^{W \rightarrow E}$	2	ps
Holes capture time from the WL into the GS, $\tau_{cp}^{W \rightarrow G}$	2	ps
Electrons reemission time from the GS to the ES, $\tau_{en}^{G \rightarrow E}$	2	ns
Electrons escape time form the ES into the WL, $\tau_{ew}^{E \rightarrow W}$	2	ns
GS spontaneous emission lifetime, τ_{rG}	1	ns
ES spontaneous emission lifetime, τ_{rE}	1	ns
WL spontaneous emission lifetime, τ_{rW}	1	ns
Stripe width, W	10	μm

2.1 Small signal analysis

We present an analytical calculation of small signal modulation (SSM) response. In order to extract the SSM response, the seven rate equations should be linearized by considering a sinusoidal current modulation

$I(t) = I_0 + I_1 e^{j\omega t}$. Thus laser values vary around their steady state solutions as follow:

$$f(t) = f_0 + f_1 e^{j\omega t} \quad (12)$$

$$s(t) = s_0 + s_1 e^{j\omega t} \quad (13)$$

To obtain the SSM response, equations (12), (13) and $I(t) = I_0 + I_1 e^{j\omega t}$ are inserted into the seven rate equations (1)-(7) and then are linearized by conniving higher order terms [26]. Both GS and ES SSM response is obtained by following calculations:

$$\begin{bmatrix} \gamma_{11} + j\omega & -\gamma_{12} & 0 & 0 & 0 & 0 & 0 \\ -\gamma_{21} & \gamma_{22} + j\omega & -\gamma_{23} & -\gamma_{24} & 0 & -\gamma_{26} & 0 \\ 0 & -\gamma_{32} & j\omega + \gamma_{33} & -\gamma_{34} & -\gamma_{35} & 0 & 0 \\ 0 & -\gamma_{42} & -\gamma_{43} & j\omega + \gamma_{44} & -\gamma_{45} & -\gamma_{46} & -\gamma_{47} \\ 0 & 0 & -\gamma_{53} & -\gamma_{54} & j\omega + \gamma_{55} & 0 & 0 \\ 0 & -\gamma_{62} & 0 & -\gamma_{64} & 0 & j\omega + \gamma_{66} & 0 \\ -\gamma_{71} & -\gamma_{72} & -\gamma_{73} & -\gamma_{74} & 0 & 0 & \gamma_{77} \end{bmatrix} \times \begin{bmatrix} f_{eWL1} \\ f_{eES1} \\ f_{eGS1} \\ f_{pGS1} \\ s_{GS1} \\ s_{ES1} \\ f_{pWL1} \end{bmatrix} = \frac{\eta_w J_1}{e N_c} \begin{bmatrix} 1 \\ 0 \\ 0 \\ 0 \\ 0 \\ 0 \\ 0 \end{bmatrix} \quad (14)$$

The GS and ES SSM responses express as:

$$\frac{\Delta S_{GS}}{\Delta J} = \frac{A_1(\omega)}{w_{1r}^2 - \omega^2 + j\gamma_1 \omega}, \quad (15)$$

$$\frac{\Delta S_{ES}}{\Delta J} = \frac{A_2(\omega)}{w_{2r}^2 - \omega^2 + j\gamma_2 \omega}, \quad (16)$$

The parameters in equations (14), (15) and (16) are introduced in appendix.

3. Results and discussions

3.1 Effect of inter-level relaxation time on light – current specifications

To investigate the effect of relaxation time on photon density, we have solved seven rate equations (1)-(7) numerically by using the fourth-order Runge-Kutta method (ODE45).

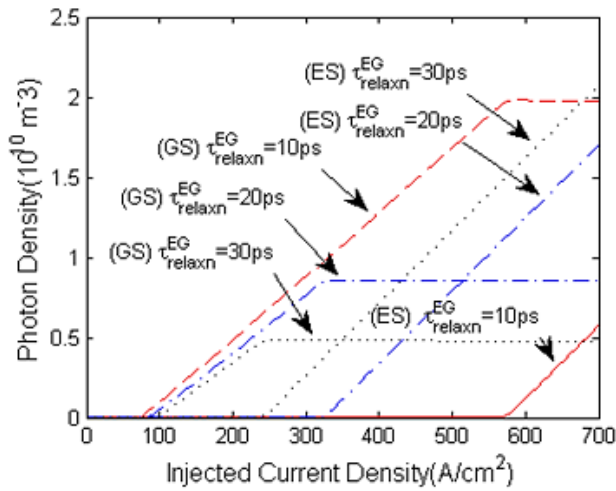


Fig. 2. Comparison of GS and ES photon density as a function of the injected current density for three relaxation times (10 ps, 20 ps and 30 ps) at 3 mm cavity length and room temperature.

Fig. 2 shows the GS and ES photon densities as a function of the injected current density with inter-level relaxation time as a parameter at room temperature (295 K). The cavity length is considered 3 mm. The numerical results show that photon density is dependent on the relaxation time. In fact, by increasing the relaxation time, the GS photon density decreases, but the ES photon density and slope efficiency increases. By increasing the relaxation time from ES to GS, the carriers slowly relax from the ES to the GS: hence the stimulated emission of ES increases. In other words, the carriers of ES emit photons when the stimulated emission of GS decreases. Therefore, the GS emission output is saturated. Such a jump of the lasing wavelength from the GS to the ES occurs by gained saturation at the GS, which is due to the phonon bottleneck and a subsequent increase in the carrier number in the ES [27]. By analysing figure 2, it should be mentioned that we are able to obtain the GS and ES threshold current density from the horizontal axis in different relaxation times.

3.2 Effect of injected current density and cavity length on SSM response

3.2.1 Effect of injected current density and cavity length on GS SSM response

Based on the transient response results, the GS SSM response is calculated from analytical expressions (14)-(52). The results for different injected current densities are shown in figures 3(a) and 3(b). The figure 3 is plotted at 10ps relaxation time from ES to GS and room temperature.

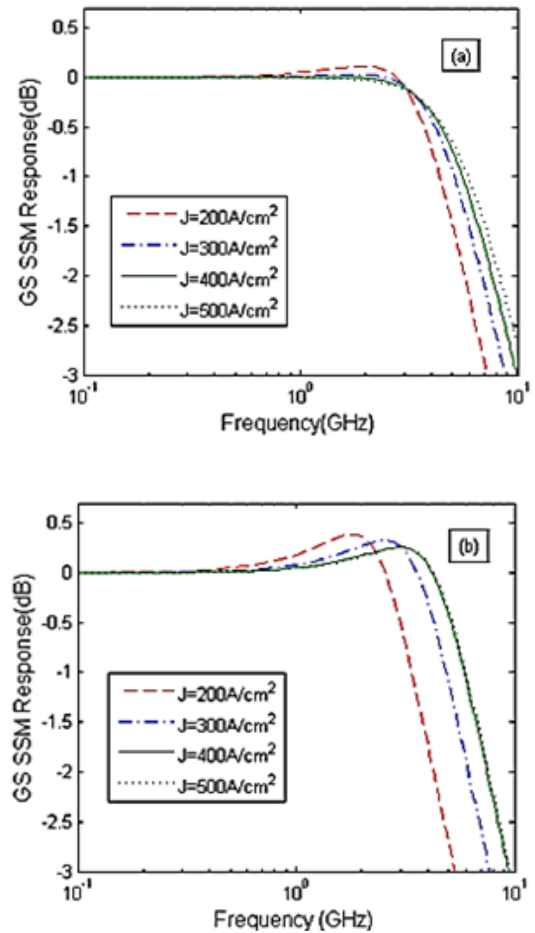


Fig. 3. GS SSM response in (a) 5 mm and (b) 2 mm cavity length at four different injected current densities, 10ps relaxation time and room temperature.

The injected current density varies from 200 to 500 A/cm^2 . For investigation of the effect of cavity length figure 3(a) is plotted in longer cavity length. In figure 3(b) the cavity length is short. As figure 3(a) and 3(b) show, the modulation bandwidth increases by increasing the current density [28].

It appears from the fact that the enhancement of injected current density causes the photon number and the relaxation oscillation frequency increase, and these causes the increase in the 3-dB modulation bandwidth. But, the relaxation oscillation amplitude decreases by increasing injected current. Further increasing the injected current density leads to increasing of the damping factor, and thus a further increase in the bandwidth is faced with limitation. In addition, by comparing figure 3(a) and 3(b), one realizes that by increasing the cavity length, the modulation bandwidth is broadened. Indeed, it is due to the inverse relation between cavity length and GS total loss. By increasing cavity length, decreasing GS total loss, increasing gain, enhancement of GS photon number and the desirable wider modulation bandwidth will be obtained.

3.2.2 Effect of injected current density and cavity length on ES SSM response

The ES SSM response is calculated from relations (16) and (53)-(60). In figure 4(a) and 4(b) ES SSM is plotted at four different injected current densities. Similarly to GS, figure 4(a) is drawn in longer cavity length and figure 4(b) in shorter cavity length.

Fig. 4(a) and 4(b) show that an increase of the injected current density leads to an increase of modulation bandwidth as we pointed in section 3.2.1. At 2mm cavity length, the ES maximum modulation bandwidth is significantly more than 5mm cavity length. By increasing cavity length, the relaxation oscillation frequency decreases. This leads to decreasing 3-dB modulation bandwidth. By comparing figure 3(a) and figure 4(b), it can also be found that the ES maximum modulation bandwidth is wider than the GS maximum modulation bandwidth. This is the high-speed modulation by ES lasing that is due to the twofold degeneracy of the ES compared to the GS. Therefore, the ES saturated gain is twice the GS saturated gain.

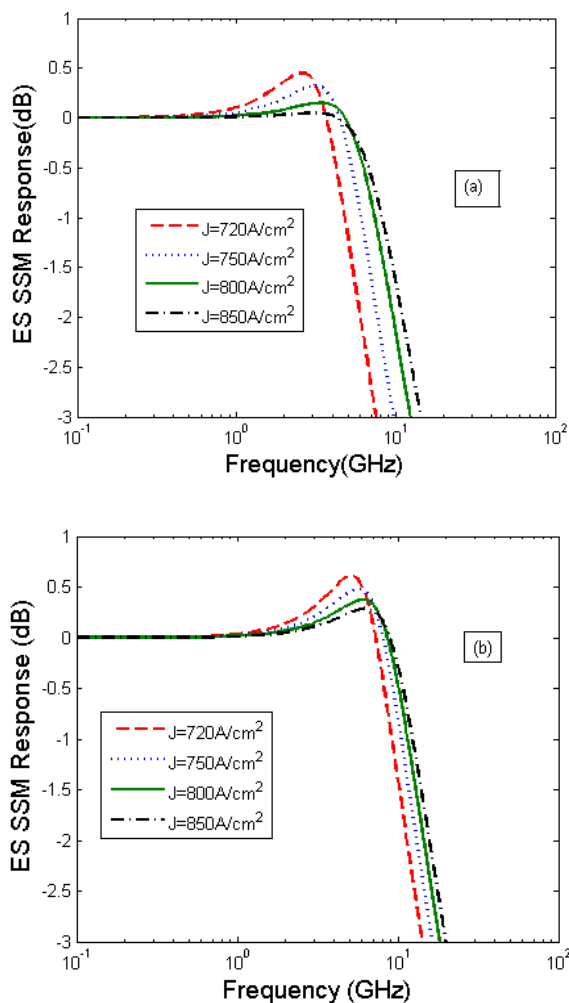


Fig. 4. ES SSM response in (a) 5mm and (b) 2mm cavity length at four different injected current densities, 10ps relaxation time and room temperature.

3.3 Effect of capture time and cavity length on SSM response

3.3.1 Effect of capture time and cavity length on GS SSM response

In fig. 5(a) and figure 5(b) the SSM responses for GS in both 5 mm and 2 mm cavity length is displayed, respectively. Capture time from the WL to the GS varies from 4ps to 30 ps. The simulation results of SSM show that the decreasing of the capture time leads to the wider the modulation bandwidth for both short and long cavity length [18, 29]. It is important to emphasize that by decreasing the capture time the relaxation oscillation frequency and relaxation oscillation amplitude increase.

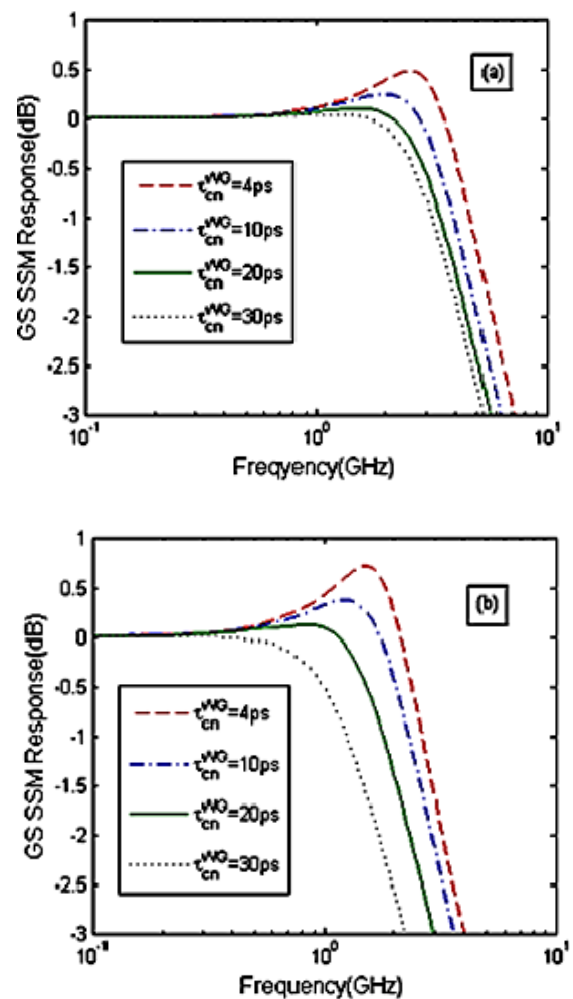


Fig. 5. GS SSM response at four different capture times in (a) 5mm and (b) 2mm cavity length.

It can be expressed that by decreasing the capture time to GS, the presence of carriers in the GS increases and so the stimulated emission of GS increases, which leads to an increase in the modulation bandwidth. By comparing fig. 5(a) and 5(b) it can be said that the 3-dB modulation bandwidth is significantly wider in longer cavity length as explained in section 3.2.1.

3.3.2 Effect of capture time and cavity length on ES SSM response

Fig. 6(a) and 6(b) show ES SSM response in three various capture times (τ_{cn}^{WE}).

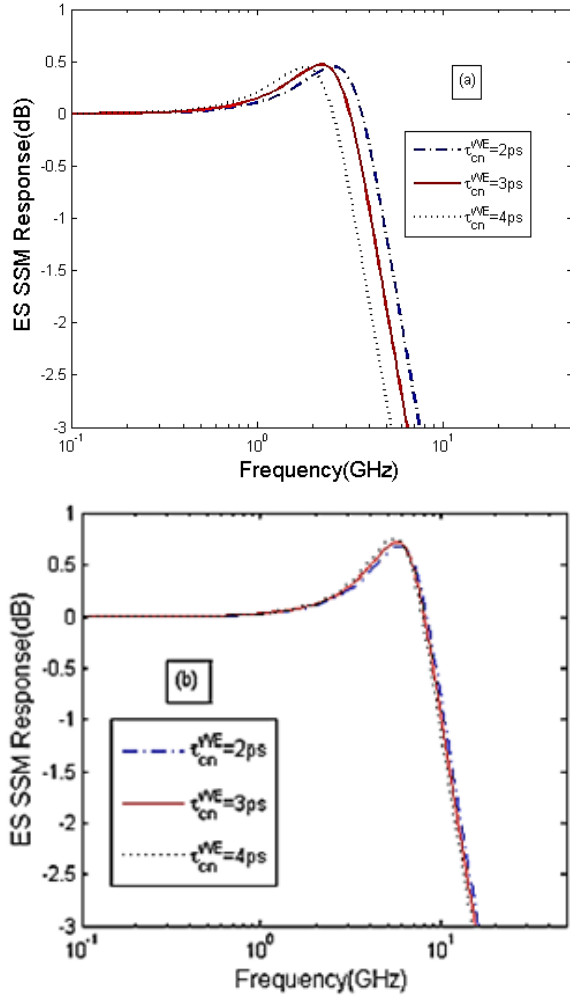


Fig. 6. ES SSM response at three different capture times in (a) 5mm and (b) 2mm cavity length.

By studying fig. 6, it can be understood that an enhancement of capture time from WL to the ES follows a decrease in the modulation bandwidth, especially in longer cavity length. This is due to a delay in the capturing of carriers into the ES and therefore a reduction of stimulated emission. In short cavity length the 3-dB modulation bandwidth is wider than the long cavity length, as we expressed in section 3.2.2. Therefore, the widest modulation bandwidth can be achieved by decreasing both the laser cavity length and the capture time from WL to the ES according to fig. 6(b).

3.4 Effect of injected current density and relaxation time on the relaxation oscillation frequency

Fig. 7(a) and 7(b) displays relaxation oscillation frequency versus the injected current density root in two

different relaxation times from ES to GS and 3 mm cavity length. One can see from figure 7 the direct relation between the injected current density root and relaxation frequency for GS and ES [26]. It should be mentioned that lower injected current density leads to a lower photon density: this is due to the fact that relaxation oscillation frequency is proportional to photon density according to relations (45)-(52) for the GS and (54)-(60) for the ES. Therefore, relaxation oscillation frequency increases by increasing the injected current density. By studying these figures, we can see the relation between relaxation oscillation frequency and relaxation time from ES to GS. As expected by increasing the relaxation time from ES to GS, GS relaxation oscillation frequency decreases while ES relaxation oscillation frequency increases. It is due to decreasing GS photon density and increasing ES photon density by increasing relaxation time. Figure 7(b) shows a non-zero relaxation oscillation frequency at low bias powers due to the carrier escape times.

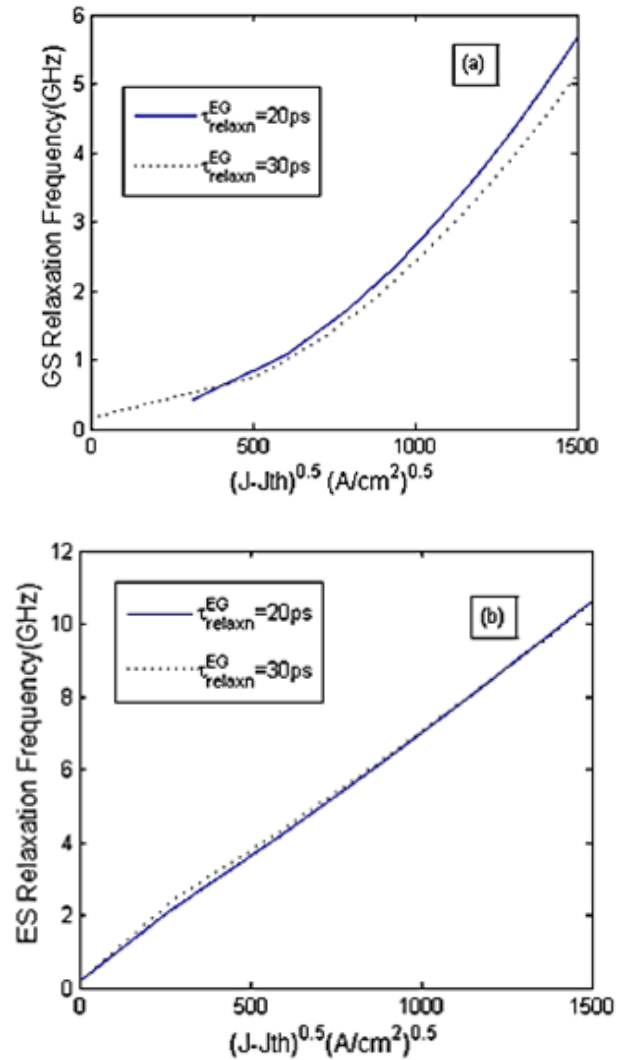


Fig. 7. Relaxation oscillation frequency as a function of the root of the injected current density at 20ps and 30ps relaxation time for (a) GS and (b) ES.

3.5 The evolution of damping factor (γ_1 and γ_2) as a function of the relaxation oscillation frequency

So far, our simulations have been based on investigation of 3-dB modulation bandwidth and high-speed characteristics. In this section, it is worthwhile to introduce the damping factor that is a limiting factor for the modulation bandwidth. Figure 8 is a plot of GS and ES damping factor versus the square of the relaxation oscillation frequency.

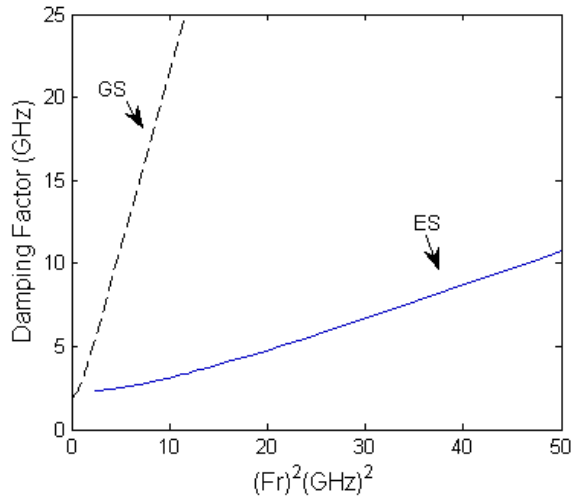


Fig. 8. GS and ES Damping factor versus square of the relaxation oscillation frequency at 3mm laser cavity length and 10ps relaxation time.

According to this figure, both damping factor and relaxation oscillation frequency have similar trends. The increase in relaxation oscillation frequency leads to an increase in the damping factor for both GS and ES. The slope of the damping factor as a function of the square of the relaxation oscillation frequency is proportional to K factor. K factor is another main factor used to determine the damping rate of a system and decreases the modulation bandwidth. Therefore, the lower rate of K factor is desirable [30]. By analysing figure 8, it is clear that the slope of the damping factor line of GS is more than the ES line. Hence, GS K factor is higher than ES K factor. Therefore, it is the high-speed modulation by ES lasing.

3.6 The evolution of damping factor (γ_1 and γ_2) as a function of the injected current density

Fig. 9 shows the effect of the injected current density on GS and ES damping factor at 10ps relaxation time and 3 mm cavity length. As expressions (50)–(60) show, the damping factor is proportional to injected current density. Enhancement of the injected current density leads to increasing the damping factor. [30]. By comparing GS and ES damping factor lines, it can be seen that the slope of GS line is more than ES: it is high-speed modulation by ES lasing.

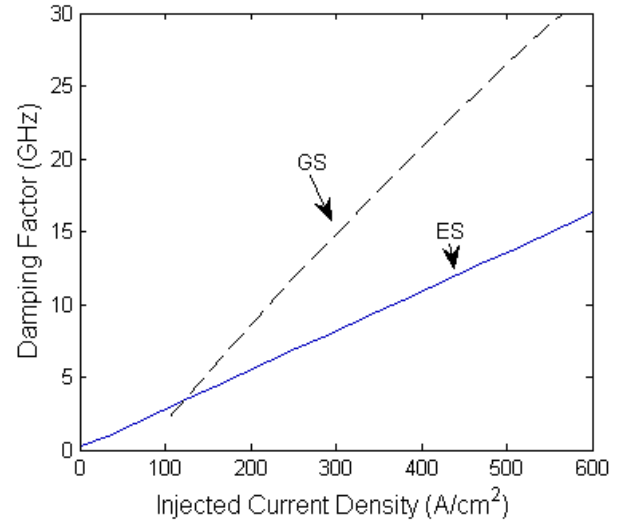


Fig. 9. Damping factor as a function of the injected current density for GS and ES.

4. Conclusion

In this paper, based on a set of rate equations for carriers and photon densities, we have theoretically calculated the SSM response function of InGaAs/GaAs QD lasers. The rate equations were solved using the fourth-order Runge-Kutta method. We have studied the light-current specifications at different inter-level relaxation times. Then, we have presented an analysis on the effect of capture time, cavity length and relaxation time on the GS and ES SSM response. The improvement of 3-dB modulation bandwidth was studied in detail. The GS bandwidth enhancement was provided by decreasing capture time and relaxation time, and increasing cavity length and injected current density. ES lasing can increase the modulation bandwidth of QD lasers at short cavity length, low capture time from WL to ES, high injected current density and high relaxation time from ES to GS. Furthermore, our studies have improved ES 3-dB modulation bandwidth to more than 10 GHz. Relaxation oscillation frequency as a function of the injected current density has been simulated. Damping factor as a function of square relaxation oscillation frequency and injected current density has been described. These phenomena show significant potential towards improving the dynamic characteristics of ES lasers as 3-dB modulation bandwidth. These results have a prime importance for further improvements in QD laser dynamic characteristics.

5. Appendix

The parameters in SSM for GS and ES (equations (15) and (16)) are presented as following equations:

$$\gamma_{11} = \frac{1 - f_{eES}^0}{\tau_{cn}^{W \rightarrow E}}, \quad (17)$$

$$\gamma_{12} = \frac{f_{eWL}^0}{\tau_{cn}^{W \rightarrow E}}, \quad (18)$$

$$\gamma_{21} = \frac{N_c}{4N_d} \frac{1 - f_{eES}^0}{\tau_{cn}^{W \rightarrow E}}, \quad (19)$$

$$\gamma_{22} = \frac{N_c}{4N_d} \frac{f_{eWL}^0}{\tau_{cn}^{W \rightarrow E}} + \frac{1 - f_{eGS}^0}{\tau_{relaxn}^{E \rightarrow G}} + 3s_{eES}^0, \quad (20)$$

$$\gamma_{23} = \frac{f_{eES}^0}{\tau_{relaxn}^{E \rightarrow G}}, \quad (21)$$

$$\gamma_{24} = -3s_{eES}^0 - \frac{6f_{eES}^0}{\tau_{rE}}, \quad (22)$$

$$\gamma_{26} = -3(f_{eES}^0 + f_{pGS}^0 - 1), \quad (23)$$

$$\gamma_{32} = 2 \frac{1 - f_{eGS}^0}{\tau_{relaxn}^{E \rightarrow G}}, \quad (24)$$

$$\gamma_{33} = \frac{2f_{eES}^0}{\tau_{relaxn}^{E \rightarrow G}} + 3s_{eGS}^0 + \frac{6f_{pGS}^0}{\tau_{rG}}, \quad (25)$$

$$\gamma_{34} = -3s_{eES}^0 - \frac{6f_{eGS}^0}{\tau_{rG}}, \quad (26)$$

$$\gamma_{35} = -3(f_{eGS}^0 + f_{pGS}^0 - 1), \quad (27)$$

$$\gamma_{42} = -2s_{eES}^0 - \frac{4f_{pGS}^0}{\tau_{rE}}, \quad (28)$$

$$\gamma_{43} = -s_{eGS}^0 - \frac{2f_{pGS}^0}{\tau_{rG}}, \quad (29)$$

$$\gamma_{44} = \frac{N_v}{6N_d} \frac{f_{pWL}^0}{\tau_{cp}^{W \rightarrow G}} + \frac{2f_{eGS}^0}{\tau_{rG}} + \frac{4f_{eES}^0}{\tau_{rE}} + s_{eGS}^0 + 2s_{eES}^0, \quad (30)$$

$$\gamma_{45} = -(f_{eGS}^0 + f_{pGS}^0 - 1), \quad (31)$$

$$\gamma_{46} = -2(f_{eES}^0 + f_{pGS}^0 - 1), \quad (32)$$

$$\gamma_{47} = \frac{N_v}{6N_d} \frac{(1 - f_{pGS}^0)}{\tau_{cp}^{W \rightarrow G}}, \quad (33)$$

$$\gamma_{53} = \frac{6N_d}{S_{GS0}} s_{eGS}^0 + \frac{12N_d \beta}{S_{GS0}} \frac{f_{pGS}^0}{\tau_{rG}}, \quad (34)$$

$$\gamma_{54} = \frac{6N_d}{S_{GS0}} s_{eGS}^0 + \frac{12N_d \beta}{S_{GS0}} \frac{f_{eGS}^0}{\tau_{rG}}, \quad (35)$$

$$\gamma_{55} = -\frac{6N_d}{S_{GS0}} (f_{eGS}^0 + f_{pGS}^0 - 1) + \frac{1}{\tau_{pG}}, \quad (36)$$

$$\gamma_{62} = \frac{12N_d}{S_{ES0}} s_{eES}^0 + \frac{24N_d \beta}{S_{ES0}} \frac{f_{pGS}^0}{\tau_{rE}}, \quad (37)$$

$$\gamma_{64} = \frac{12N_d}{S_{ES0}} s_{eES}^0 + \frac{24N_d \beta}{S_{ES0}} \frac{f_{eES}^0}{\tau_{rE}}, \quad (38)$$

$$\gamma_{66} = -\frac{12N_d}{S_{ES0}} (f_{eES}^0 + f_{pGS}^0 - 1) + \frac{1}{\tau_{pE}}, \quad (39)$$

$$\gamma_{71} = \frac{N_c}{2N_d}, \quad (40)$$

$$\gamma_{72} = 2, \quad (41)$$

$$\gamma_{73} = 1, \quad (42)$$

$$\gamma_{74} = 3, \quad (43)$$

$$\gamma_{77} = \frac{N_v}{2N_d}. \quad (44)$$

$$A_1(w) = \frac{r_1 \eta_w}{2eN_d} \left(1 + \frac{\tau_{cn}^{WE}}{3\tau_{cp}^{WG}} \frac{(1 - f_{pGS}^0)}{(1 - f_{eES}^0)} \right) + \frac{r_1 \eta_w}{jw2eN_d} \left(Q_1 - \frac{4\tau_{cn}^{WE}}{3\tau_{cp}^{WG}} \frac{(1 - f_{pGS}^0)}{(1 - f_{eES}^0)} \frac{f_{eES}^0}{\tau_{rE}} \right) + \frac{(1 - f_{pGS}^0)}{3\tau_{cp}^{WG}} - \frac{\alpha_1}{3}, \quad (45)$$

$$r_1 = \frac{6N_d}{S_{GS0}} s_{eGS}^0, \quad (46)$$

$$\alpha_1 = 3s_{eGS}^0 + 6 \frac{f_{pGS}^0}{\tau_{rG}} \quad (47)$$

$$Q_1 = \frac{N_v}{6N_d} \frac{f_{pWL}^0}{\tau_{cp}^{WG}} + \frac{(1-f_{pGS}^0)}{\tau_{ep}^{WG}} + \frac{2f_{eGS}^0 S_{GS}^0}{\tau_{rG}} + \frac{4f_{eES}^0}{\tau_{rE}} \quad (48)$$

w_{1r} is relaxation oscillation frequency and γ_1 is damping factor that are given as:

$$w_{1r}^2 = \frac{B_1}{jw}, \quad (49)$$

$$\gamma_1 = Q_1 + \alpha_1 + Z_1 / jw, \quad (50)$$

In equations (49) and (50) B_1 and Z_1 are written as:

$$B_1 = 3r_1 Q_1 (f_{eGS}^0 + f_{pGS}^0 - 1) - \frac{12f_{eES}^0 r_1 (f_{eGS}^0 + f_{pGS}^0 - 1)}{\tau_{rE}} + \quad (51)$$

$$r_1 (f_{eGS}^0 + f_{pGS}^0 - 1) \frac{(1-f_{pGS}^0)}{\tau_{cp}^{WG}} -$$

$$r_1 \alpha_1 (f_{eGS}^0 + f_{pGS}^0 - 1),$$

$$Z_1 = \alpha_1 Q_1 + 4r_1 (f_{eGS}^0 + f_{pGS}^0 - 1) + \left(\alpha_1 + \frac{12f_{eES}^0}{\tau_{rE}} \right) \frac{(1-f_{pGS}^0)}{3\tau_{cp}^{WG}} - \frac{\alpha_1}{3} \left(\alpha_1 + \frac{12f_{eES}^0}{\tau_{rE}} \right). \quad (52)$$

We can obtain the ES small signal modulation response as the way calculated for GS by:

$A_2(w)$, relaxation oscillation frequency and damping factor of excited state can be written respectively as:

$$A_2(w) = \frac{\eta_w r_2 Q_2}{4eN_d} + \frac{\eta_w r_2 Q_2}{4eN_d} (-2\alpha_2 + \frac{N_c}{6N_d} \frac{(1-f_{pGS}^0)}{(1-f_{eES}^0)} \frac{f_{eWL}^0}{\tau_{cp}^{WG}} + \frac{2}{3} \left(\frac{1-f_{pGS}^0}{\tau_{cp}^{WG}} \right) - \frac{\eta_w r_2}{2eN_d} \frac{\tau_{cn}^{WE}}{\tau_{cp}^{WG}} \frac{(1-f_{pGS}^0)}{(1-f_{eES}^0)} \frac{f_{eGS}^0}{\tau_{rG}}), \quad (53)$$

$$w_{2r}^2 = \frac{1}{jw} (3p_2 r_2 Q_2 + 3p_2 r_2 (-2\alpha_2 + \frac{N_c}{6N_d} \frac{(1-f_{pGS}^0)}{(1-f_{eES}^0)} \frac{f_{eWL}^0}{\tau_{cp}^{WG}} + \frac{2}{3} \left(\frac{1-f_{pGS}^0}{\tau_{cp}^{WG}} \right) -$$

$$6p_2 r_2 \frac{f_{eGS}^0}{\tau_{rG}})), \quad (54)$$

$$\gamma_2 = Q_2 + 3\alpha_2 + \frac{Z_2}{jw}, \quad (55)$$

$$Q_2 = \frac{N_v}{6N_d} \frac{f_{pWL}^0}{\tau_{cp}^{WG}} + \frac{(1-f_{pGS}^0)}{\tau_{cp}^{WG}} + \frac{4f_{eES}^0}{\tau_{rE}} + 2 \frac{f_{eGS}^0}{\tau_{rG}} + 2S_{ES}^0, \quad (56)$$

$$r_2 = \frac{12N_d}{SES_0} S_{ES}^0, \quad (57)$$

$$P_2 = f_{eGS}^0 + f_{pGS}^0 - 1, \quad (58)$$

$$\alpha_2 = S_{ES}^0 + \frac{2f_{pGS}^0}{\tau_{rE}}, \quad (59)$$

$$Z_2 = \frac{1}{jw} (3\alpha_2 Q_2 + 5p_2 r_2 + 3(\alpha_2 + \frac{f_{eGS}^0}{\tau_{rG}}) (-2\alpha_2 + \frac{N_c}{6N_d} \frac{(1-f_{pGS}^0)}{(1-f_{eES}^0)} \frac{f_{eWL}^0}{\tau_{cp}^{WG}} + \frac{2}{3} \left(\frac{1-f_{pGS}^0}{\tau_{cp}^{WG}} \right)). \quad (60)$$

References

- [1] G. T. Liu, A. Stintz, H. Li, K. J. Malloy, L. F. Lester. *Electron. Lett.* **35**, 1163 (1999).
- [2] S. S. Mikhrin, A. R. Kovsh, I. L. Krestnikov, A. V. Kozhukhov, D. A. Livshits, N. N. Ledentsov, Y. M. Shernyakov, I. I. Novikov, M. V. Maximov, V. M. Ustinov, Z. I. Alferov. *Semicond. Sci. Technol.* **20**, 340 (2005).
- [3] H. Saito, K. Nishi, A. Kamei, S. Sugou. *IEEE Photon. Technol. Lett.* **12**, 1298 (2000).
- [4] D. L. Huffaker, G. Park, Z. Zou, O. B. Shchekin, D. G. Deppe. *Appl. Phys. Lett.* **73**, 2564 (1998).
- [5] O. B. Shchekin, D. G. Deppe. *Appl. Phys. Lett.* **80**, 2758 (2002).
- [6] D. G. Deppe, H. Huang, O. B. Shchekin. *IEEE J. Quantum Electron.* **38**, 1587 (2002).

- [7] D. G. Deppe, H. Huang. *IEEE J. Quantum Electron.* **42**, 324 (2006).
- [8] D. G. Deppe, D. L. Huffaker. *Appl. Phys. Lett.* **77**, 3325 (2000).
- [9] M. Ishida, N. Hatori, T. Akiyama, K. Otsubo, Y. Nakata, H. Ebe, M. Sugawara, Y. Arakawa. *Appl. Phys. Lett.* **85**, 4145 (2004).
- [10] M. Ishida, N. Hatori, T. Akiyama, K. Otsubo, Y. Nakata, H. Ebe, M. Sugawara, Y. Arakawa. presented at the Int. Conf. Indium Phoshide Related Mater (2004).
- [11] A. V. Uskov, Y. Boucher, J. L. Bihan, J. McInerney. *Appl. Phys. Lett.* **73**, 1499 (1998).
- [12] E. Malic, K. J. Ahn, M. J. P. Bormann, P. Hövel, E. Schöll, A. Knorr, M. Kuntz, D. Bimberg. *Appl. Phys. Lett.* **89**, 101107-1 (2006).
- [13] A. Fiore, A. Markus. *IEEE J. Quantum Electron.* **43**, 287 (2007).
- [14] P. Bhattacharya, D. Klotzkin, O. Qasaimeh, W. Zhou, S. Krishna, D. Zhu. *IEEE J. Sel. Top. Quantum Electron.* **6**, 426 (2000).
- [15] P. Bhattacharya, S. Ghosh, S. Pradhan, J. Singh, Z. K. Wu, J. Urayama, K. Kim, T. B. Norris. *IEEE J. Quantum Electron.* **39**, 952 (2003).
- [16] L. Zhang, T. F. Boggess, D. G. Deppe, D. L. Huffaker, O. B. Shchekin, C. Cao. *Appl. Phys. Lett.* **76**, 1222 (2000).
- [17] T. F. Boggess, L. Zhang, D. G. Deppe, D. L. Huffaker, C. Cao. *Appl. Phys. Lett.* **78**, 276 (2001).
- [18] F. Grillot, C. Wang, N. Naderi, J. Even. *IEEE J. Quantum Electron.* **19**, 1900 (2013).
- [19] C. Tong, D. Xu, S. F. Yoon. *Lightwave Technology J.* **27**, 5442 (2009).
- [20] D. G. Deppe, H. Huang. *IEEE J. Quantum Electron.* **42**, 324 (2006).
- [21] L.W. Shi, Y. H. Chen, B. Xu, Z. C. Wang. *Physica E.* **39**, 203 (2007).
- [22] G. A. Narvaez, G. Bester, A. Zunger. *Phys. Rev. B.* **74**, 075403 (2006).
- [23] J. Urayama, T. B. Norris, J. Singh. *Phys. Rev. Lett.* **86**, 4930 (2001).
- [24] T. Müller, F. F. Schrey, G. Strasser, K. Unterrainer. *Appl. Phys. Lett.* **83**, 3572 (2003).
- [25] M. D. Giorgi, C. Lingk, G. Plessen. *Appl. Phys. Lett.* **79**, 3968 (2001).
- [26] C. Wang, F. Grillot, J. Even. *IEEE. Quantum Electron.* **48**, 1144 (2012).
- [27] M. H. Yavari, V. Ahmadi. *IEEE. Quantum Electron.* **15**, 774 (2009).
- [28] X. Jin, T. Keating, S. L. Chuang. *IEEE. Quantum Electron.* **36**, 1485 (2000).
- [29] L. V. Asryan, W. Yuchang, R. A. Suris. *Appl. Phys. Lett.* **98**, 131108 (2011).
- [30] R. R. Alexander, D. T. D. Childs, H. Agarwal, K. M. Groom, H. Y. Liu, M. Hopkinson, R. A. Hogg, M. Ishida, T. Yamamoto, M. Sugawara, Y. Arakawa, T. J. Badcock, R. J. Royce, D. J. Mowbray. *IEEE J. Quantum Electron.* **43**, 1129 (2007).

*Corresponding author: raf404@guilan.ac.ir